Higher-order dispersion and nonlinear effects of optical fibers under septic self-steepening and self-frequency shift

Karabo K. Ndebele,[1,*] Conrad B. Tabi,[1,†] Camus G. Latchio Tiofack,[2,‡] and Timoléon C. Kofané[1,2,3,§]

[1]*Department of Physics and Astronomy, Botswana International University of Science and Technology, Private Mail Bag 16 Palapye, Botswana*

[2]*Department of Physics, Laboratory of Mechanics, Faculty of Science, University of Yaoundé I, P.O. Box 812, Yaoundé, Cameroon*

[3]*Centre d'Excellence Africain en Technologies de l'Information et de la Communication, University of Yaoundeì I, P.O. Box 812, Yaounde, Cameroon*

(Received 5 December 2020; revised 18 August 2021; accepted 4 October 2021; published 19 October 2021)

We investigate the modulational instability (MI) of a continuous wave (cw) under the combined effects of higher-order dispersions, self steepening and self-frequency shift, cubic, quintic, and septic nonlinearities. Using Maxwell's theory, an extended nonlinear Schrödinger equation is derived. The linear stability analysis of the cw solution is employed to extract an expression for the MI gain, and we point out its sensitivity to both higher-order dispersions and nonlinear terms. In particular, we insist on the balance between the sixth-order dispersion and nonlinearity, septic self-steepening, and the septic self-frequency shift terms. Additionally, the linear stability analysis of cw is confronted with the stability conditions for solitons. Different combinations of the dispersion parameters are proposed that support the stability of solitons and the occurrence of MI. This is confronted with full numerical simulations where the input cw gives rise to a broad range of behaviors, mainly related to nonlinear patterns formation. Interestingly, under the activation of MI, a suitable balance between the sixth-order dispersion and the septic self-frequency shift term is found to highly influence the propagation direction of the optical wave patterns.

DOI: 10.1103/PhysRevE.104.044208

I. INTRODUCTION

The study of exact traveling wave solutions plays a vital role to understand the nonlinear physical phenomena of nonlinear evolution equations, which exist in many areas of science, such as plasma physics, fluid dynamics, nonlinear optics, elastic media, optical fibers, hydrodynamics, biology, and many more [1–5]. Optical solitons have been an active topic of research during the past decades because of their potential applications in long-distance communication [6,7]. The pioneering works of Hasegawa and Tappert [8,9], who predicted solitons theoretically, and Mollenauer *et al.* [10,11], who observed them experimentally, made solitons a practical tool for data transmission. There has been much interest in recent years in the supercontinuum generation in optical fibers because of their high potential for applications in the fields of optical communications [12], generation of ultrashort pulses [13] in highly nonlinear dispersion-shifted fibers [14] using picosecond or femtosecond laser pulses with high peak power. It is well known that the standard nonlinear Schrödinger (NLS) equation can be used to describe the propagation of a picosecond optical pulse. However, higher-order effects, such as the third-order dispersion (TOD), fourth-order dispersion (FOD), fifth-order dispersion (FFOD), sixth-order dispersion (SOD), which should be considered when the pulse width is below 10 fs [15–17], higher-order nonlinearities (should not be neglected when the optical field frequency approaches a resonant frequency of the optical fiber materials [17,18]), self-steepening (SS), and self-frequency shift (SFS) induced by Raman stimulated scattering are indispensable for describing the propagation of ultrashort pulses [19–22]. In the picosecond systems, the NLS equation is the central governing pulse envelope equation in which the self-phase modulation and the group-velocity dispersion (GVD) effects are just taken into description [23]. It is well known that as the intensity of the incident light field becomes stronger, non-Kerr nonlinear effects become important [18,24], and the NLS family of equations should describe the dynamics of the pulses with higher-order nonlinear terms [25–31] from which can emerge a new class of soliton solutions. One of the key issues of soliton theory is the universal modulational instability (MI) phenomenon, which leads to the emergence of localized coherent nonlinear structures and the formation of trains of soliton pulses.

MI is a fundamental and ubiquitous nonlinear phenomenon that pertains to a large variety of subfields of physics, such as fluid dynamics [2], plasma physics [32], atomic physics (atomic Bose-Einstein condensates), and nonlinear optics [33]. MI implies that as a result of the combined action of the group velocity dispersion (GVD) or the second-order chromatic dispersion and self-phase modulation (SPM) or the self-focusing Kerr nonlinearity of the medium, amplitude, or phase perturbations added to a continuous or quasicontinuous

*karabo.ndebele@studentmail.biust.ac.bw
†Corresponding author: tabic@biust.ac.bw
‡glatchio@yahoo.fr
§tckofane@yahoo.com

wave (cw) exhibit exponential growth. This is accompanied by sideband evolution with a frequency separation from the carrier, proportional to its power. In the anomalous dispersion regime, that is, when we use optical fiber with negative GVD, the dominant unstable MI frequencies can be shown to be proportional to the cw amplitude and inversely proportional to the square root of the dispersion [15,17]. Thus, the modulation that grows on the cw field increases frequency as the dispersion goes to zero. Even in the normal dispersion regime, MI can occur due to third- and fourth-order dispersion corrections [34]. In addition, various higher-order linear and nonlinear effects, such as higher dispersions, self-steepening, and time-delayed Raman effects have also been considered, and these effects are found to influence MI in optical fibers strongly [35,36]. In optics, MI has constituted a wide field of intense theoretical and experimental research including ultrafast pulse generation [37], supercontinuum generation [38,39], four-wave mixing (FWM) [40,41], Bragg gratings [42], parametric oscillators [43,44], and optical fiber systems [45–48]. In the meantime, many research activities have been carried to understand and characterize optical soliton under: (i) strong nonlinearity versus weak dispersion [49], (ii) strong dispersion versus weak nonlinearity [34,50], and (iii) a subtle balance between dispersion and nonlinearity with the main objective being the generation of solitary waves. Our paper relies on the third stream. We hope that a sixth-order linear dispersion and sixth-order nonlinear dispersions can suitably balance septic nonlinearity and lead to the formation of nonlinear structures. In our contribution, we start with Maxwell's equations describing the response of the nonlinear medium to electromagnetic waves. Then we report on the derivation of the one plus one dimensional [(1 + 1)D] cubic-quintic-septic NLS equation with third-, fourth-, fifth-, and sixth-order dispersions. Furthermore, we examine theoretically and numerically MI of few-cycle pulses using linear stability analysis of linearized equations for small perturbations and using direct numerical simulation to support our analytical predictions.

The rest of the paper is organized as follows. In Sec. II, we derive a (1 + 1)D cubic-quintic-septic NLS equation describing the dynamics of ultrashort pulses in nonlinear optical fibers under the combined effects of dispersion, loss, gain, cubic, and cubic-quintic-septic nonlinearities, and cubic-quintic-septic self-steepening and self-frequency shift terms, respectively. In Sec. III, the linear stability analysis of the MI is addressed, and instability zones, as well as the analytic expressions of the gain of MI, are obtained. Based on analytical findings, numerical simulations are carried out on the (1 + 1)D cubic-quintic-septic NLS equation using the split-step Fourier method. Particular attention is paid to the combined effects of the sixth-order dispersion cubic, quintic, septic self-steepening, and self-frequency shift parameters. Some concluding remarks are given in Sec. V.

II. DERIVATION OF THE HIGHER-ORDER NONLINEAR SCHRÖDINGER EQUATION

We consider the cubic-quintic-septic nonlinearities of nonlinear medium, which arise from the expansion of the refractive index in the power series of intensity I of the light pulse,

$$n_f(\omega) = n_0 + n_2 I + n_4 I^2 + n_6 I^3. \tag{1}$$

Here, n_0 is the linear refractive index coefficient, and n_2, n_4, and n_6 are the nonlinear refractive index coefficients, which originate from third-, fifth-, and seventh-order susceptibility, respectively, $I = |E|^2$, E being the electric field vector. The complex dielectric constant, related to optical signal propagation through an optical fiber is as follows:

$$\varepsilon(\omega) = n_f^2(\omega) = n_0^2 + 2n(\omega)\Delta n, \tag{2}$$

with Δn being given by

$$\Delta n = n_2|E|^2 + \left[\frac{n_0^2}{2} + n_4\right]|E|^4 + \left[n_6 + \frac{n_2 n_4}{n_0}\right]|E|^6. \tag{3}$$

Following Agrawal [17], the propagation equation for $\tilde{\psi}(z, \omega - \omega_0)$, which is the Fourier transform of $\psi(z, t)$, is written in the form

$$\frac{\partial \tilde{\psi}}{\partial z} = i[\beta(\omega) + \Delta\beta - \beta_0]\tilde{\psi}, \tag{4}$$

where $\beta(\omega)$ is Taylor's expansion in series, up to sixth-order, about the carrier frequency and the quantity $\Delta\beta$ is defined as

$$\Delta\beta = k_0 \frac{\int_{\infty}^{-\infty}\int_{\infty}^{-\infty} \Delta n|f(x,y)|^2 dx\, dy}{\int_{\infty}^{-\infty}\int_{\infty}^{-\infty} |f(x,y)|^2 dx\, dy}, \tag{5}$$

with k_0 as the wave number and $f(x, y)$ being the modal distribution of the fundamental mode of the optical fiber. We should note that nonlinearities relative to the self-steepening and self-frequency shift are modeled through the propagation constant. Taking the inverse Fourier transform of Eq. (4), we obtain the following envelope equation for ultrashort pulses in optical fiber:

$$\begin{aligned} i\psi_z + \sum_{m=2}^{6}(i)^m \partial_t^m \psi + \left(\sum_{m=1}^{3}\gamma_m|\psi|^{2m}\right)\psi \\ + i\sum_{m=1,3,5}\alpha_m(|\psi|^{m+1}\psi)_t \\ + \sum_{m=2,4,6}\alpha_m(|\psi|^m)_t\psi = 0, \end{aligned} \tag{6}$$

where $\partial_t^m = \frac{\partial^m}{\partial t^m}$. More precisely, $\psi(z, t)$ is the envelope amplitude of the electric field, t is the retarded time frame, and z is the propagation distance originating from the transformation, $T = t - z/v_g = t - \beta_1$. All the coefficients are real constants. The above equation is a higher-order NLS equation with higher-order dispersion and cubic, quintic, and septic non-Kerr nonlinearities. γ_1, γ_2, and γ_3 are the cubic, quintic, and septic nonlinearities, respectively, whereas α_1, α_3, and α_5 are the cubic, quintic, and septic self-steepening terms, respectively. The terms α_2, α_4, and α_6 are the cubic, quintic, and septic self-frequency shift induced by stimulated Raman scattering, respectively. β_2 is the GVD term, β_3 is the TOD term, β_4 is the FOD, β_5 is the FFOD term, and β_6 is the SOD term. The expressions of parameters in Eq. (6) are given in the Appendix. Recent advances in the fabrication of photonic-crystal

fibers (PCFs) [51–54] have made possible the production of small-core PCFs where strong nonlinear interactions occur at relatively low peak powers and over short propagation distances. The FWM theory has been developed, which goes beyond the slowly varying envelope approximation of the NLS equation and is based on the full wave equation, allowing the rigorous study of the left-most instability band (the first FWM peak) and the far-detuned instability peak (the secondary FWM). In this approach, the perturbation wave numbers are the roots of the fourth-order algebraic equation [55] where the two extra roots can describe excitation of both forward and backward waves. At the same time, all previous results on FWM in fibers with nontrivial dispersion characteristics resulted in a quadratic equation for the perturbation wave numbers [17,56–59]. These two extra roots have negative imaginary parts, generating instabilities [55]. In general, the first FWM peak, which has a direct analog in the idealized NLS equation in the anomalous dispersion regime, corresponds to a wave with a Stokes component slightly stronger than the anti-Stokes one, and the second peak, which appears in the model due to modified fiber dispersion, and which does not exist in the idealized NLS, generates a stronger anti-Stokes wave. In the meantime, a generalized NLS equation has been derived, including self-steepening effects, whereas the summation characterizing higher-order dispersion is taken up to order $N = 20$, high enough to ensure that the dispersion profile is adequately approximated in the frequency domain under consideration [55]. It has been, however, pointed out that the generalized NLS equation is often insufficient for quantitative comparisons between experimental and theoretical results since the dependence of the nonlinearity on the detuning parameter is taken into only approximately [55]. Indeed, the existence of the second FWM peak is ensured by positive higher-order dispersion terms greater or equal to 6, namely, the positive dispersions of orders two, four, and six, respectively, and requires sufficiently large values of the detuning parameter because higher-order dispersions terms are very small. However, due to extra degrees of freedom, PCFs allow mode propagation to be easily manipulated. They are made of an array of microscopic air holes distributed throughout their entire length that surrounds a pure silica core. Therefore, nonlinear effects are enhanced due to light concentration into a very small area between silica and air, and their balance with higher-order dispersions can be used to explain optical pulse communication in highly nonlinear photonic crystal fiber, which imposes to extend the order of nonlinear terms in the standard NLS equation beyond Kerr nonlinearity.

In order to simplify the problem at hand, it would be advisable to reduce the number of parameters. Therefore, Eq. (6) can be normalized by making use of the transformations $Z = z/L_D$ for space, $\tau = t/T_0$ for time and $u = \frac{\psi}{\sqrt{P_0}}N$ for amplitude, which leads to the following normalized HNLS equation:

$$\begin{aligned} iu_Z &+ \sum_{m=2}^{6}(i)^m k_m \partial_\tau^m u + n_{NL}|u|^2u + n_{NL4}|u|^4u \\ &+ n_{NL6}|u|^6u + in_{\rm SS}(|u|^2u)_\tau + in_{\rm SS4}(|u|^4u)_\tau \\ &+ in_{\rm SS6}(|u|^6u)_\tau + n_{\rm SFS}(|u|^2)_\tau u \\ &+ n_{\rm SFS4}(|u|^4)_\tau u + n_{\rm SFS6}(|u|^6)_\tau u = 0, \end{aligned} \tag{7}$$

where

$$\begin{aligned} &k_2 = \mathrm{sgn}(\beta_2), \quad k_m = \sum_{m=3}^{6}\frac{L_D}{L_{Dm}}, \quad n_{\rm NL} = \frac{L_D}{L_{\rm NL}N^2}, \\ &n_{\rm NL4} = \frac{L_D}{L_{\rm NL4}N^4}, \quad n_{\rm NL6} = \frac{L_D}{L_{\rm NL6}N^6}, \quad n_{\rm SS} = \frac{L_D}{L_{\rm SS}N^2}, \\ &n_{\rm SS4} = \frac{L_D}{L_{\rm SS4}N^4}, \quad n_{\rm SS6} = \frac{L_D}{L_{\rm SS6}N^6}, \quad n_{\rm SFS} = \frac{L_D}{L_{\rm SFS}N^2}, \\ &n_{\rm SFS4} = \frac{L_D}{L_{\rm SFS4}N^4}, \quad n_{\rm SFS6} = \frac{L_D}{L_{\rm SFS6}N^6}, \end{aligned} \tag{8}$$

with $L_D = \frac{T_0^2}{\beta_2}$, $L_{Dm} = \sum_{m=3}^{6}\frac{T_0^m}{\beta_m}$, $N^2 = \frac{L_D}{L_{\rm NL}}$, $L_{\rm NL} = \frac{1}{\gamma_1 P_0}$, $L_{\rm NL4} = \frac{1}{\gamma_2 P_0^2}$, $L_{\rm NL6} = \frac{1}{\gamma_3 P_0^3}$, $L_{\rm SS} = \frac{T_0}{\alpha_1 P_0}$, $L_{\rm SS4} = \frac{T_0}{\alpha_3 P_0^2}$, $L_{\rm SS6} = \frac{T_0}{\alpha_5 P_0^3}$, $L_{\rm SFS} = \frac{T_0}{\alpha_2 P_0}$, $L_{\rm SFS4} = \frac{T_0}{\alpha_4 P_0^2}$, $L_{\rm SFS6} = \frac{T_0}{\alpha_6 P_0^3}$. The above quantities are dimensionless parameters depending on the typical values [60–62]: $P_0 = 10$ W, $\beta_6 = 0.5$ ps^6 m^{-1}, $\beta_5 = 0.001\,23$ ps^5 m^{-1}, $\beta_4 = 10$ ps^4 m^{-1}, $\beta_3 = 0.009$ ps^3 m^{-1}, $\beta_2 = 50$ ps^2 m^{-1}, $\gamma_1 = 1$ kW^{-1} m^{-1}, $\gamma_2 = 1$ kW^{-2} m^{-1}, $\gamma_3 = 0.031$ kW^{-1} m^{-3}, $\alpha_1 = -0.0247$ kW^{-1}/[(2π)mTHz], $\alpha_2 = 0.037\,05$ kW^{-1}psm^{-1}, $\alpha_3 = -0.0247$ kW^{-2}/[(2π) mTHz], $\alpha_4 = -0.030\,875$ kW^{-2}psm^{-1}, $\alpha_5 = 0.004$ kW^{-3}/[(2π) mTHz] and $\alpha_6 = 0.02$ kW^{-3} psm^{-1}.

The advantage of deriving the above higher-order nonlinear Schrödinger equation (HNLS) equation is that we see the mathematical input of the aforementioned respective nonlinearities that most researchers do not show. The model we have presented has a set of new parameters compared to the previous papers [31,63–65]. Before ending, let us mention that the self-steepening and self-frequency shift terms have been taken into account in optical fibers whose pulse dynamics are well described by the complex Ginzburg-Landau equation [46,66,67]. Our HNLS equation governs the dynamics of ultrashort pulses where septic self-steepening and self-frequency shift terms come into action. The existence of solitons in an optical fiber system described by the HNLS equation further requires the balance among self-steepening and self-frequency shift effects also called the derivative Kerr nonlinear terms. The balance among the derivative quintic non-Kerr nonlinear terms and the balance between the derivative septic non-Kerr nonlinear terms are all accounted for in Eq. (7). It is remarked that such balance aspects are also required for the formation of ultrashort soliton pulses [68].

III. MODULATIONAL INSTABILITY

A. Linear stability analysis and gain spectrum

The MI is studied on model Eq. (7) via the linear stability analysis of a CW solution, which propagates inside the optical fiber with the initial input power P_0, i.e.,

$$u(Z,\tau) = \sqrt{P_0}e^{i\phi_{\rm NL}}, \tag{9}$$

where $\phi_{\rm NL} = n_{\rm NL}P_0 + n_{\rm NL4}P_0^2 + n_{\rm NL6}P_0^3$ is the nonlinear phase shift due to the self-phase modulation and higher-order

nonlinear terms. The stability of solution (9) requires the introduction of slight perturbation so that

$$u(Z,\tau) = [\sqrt{P_0} + a(Z,\tau)]e^{i\phi_{\rm NL}}, \tag{10}$$

where $a(Z,\tau)$ is the small perturbation with $|a(Z,\tau)| \ll \sqrt{P}$ being the complex field. This perturbed solution means that if the perturbed field grows exponentially, the steady state will become unstable. Substituting Eq. (10) in Eq. (7), and linearizing around the unperturbed solution, leads to the following equation for the perturbed field:

$$\begin{aligned} & ia_Z - k_2 a_{\tau\tau} - ik_3 a_{\tau\tau\tau} + k_4 a_{\tau\tau\tau\tau} \\ & + ik_5 a_{\tau\tau\tau\tau\tau} - k_6 a_{\tau\tau\tau\tau\tau\tau} + n_{NL}[P_0(a+a^*)] \\ & + n_{\rm NL4}[2P_0^2(a+a^*)] + n_{\rm NL6}[3P_0^3(a+a^*)] \\ & + in_{\rm SS}[2P_0 a_\tau + P_0 a_t^*] + in_{\rm SS4}P_0^2[3a_\tau + 2a_\tau^*] \\ & + in_{\rm SS6}P_0^3[4a_\tau + 3a_\tau^*] + n_{\rm SFS}P_0[a_\tau + a_\tau^*] \\ & + 2n_{\rm SFS4}P_0^2[a_\tau + a_\tau^*] + 3n_{\rm SFS6}P_0^3[a_\tau + a_\tau^*] = 0, \end{aligned} \tag{11}$$

where a^* is the complex conjugate of the perturbed field. Furthermore, solution for Eq. (11) can be adopted in the form

$$a(Z,\tau) = u(Z)e^{-i\Omega\tau} + v(Z)e^{i\Omega\tau}, \tag{12}$$

where $u(Z)$ and $v(Z)$ are the complex perturbation fields and Ω is the complex modulation frequency. Making use of the ansatz of the perturbed field of Eq. (12) in the linearized Eq. (11) leads to a 2×2 matrix of the following form for the perturbed fields:

$$i\frac{\partial}{\partial s}\begin{pmatrix} u(Z) \\ v^*(Z)\end{pmatrix} = \begin{pmatrix} T_{11} & T_{12} \\ T_{21} & T_{22}\end{pmatrix}\begin{pmatrix} u(Z) \\ v^*(Z)\end{pmatrix}, \tag{13}$$

where $v^*(Z)$ is the complex conjugate of the field $v(Z)$ with the matrix elements being given by

$$\begin{aligned} T_{11} &= -\big[k_2\Omega^2 + k_3\Omega^3 + ka_4\Omega^4 + k_5\Omega^5 + k_6\Omega^6 + m \\ &\quad + \Omega P_0\big(2n_{\rm SS} + 3n_{\rm SS4}P_0 + 4n_{\rm SS6}P_0^2 \\ &\quad - in_{\rm SFS} - 2in_{\rm SFS4}P_0 - 3in_{\rm SFS6}P_0^2\big)\big], \\ T_{12} &= -\big[m + \Omega P_0\big(n_{\rm SS} + 2n_{\rm SS4}P_0 + 3n_{\rm SS6}P_0^2 \\ &\quad - in_{\rm sFS} - 2in_{\rm SFS4}P_0 - 3in_{\rm SFS6}P_0^2\big)\big], \\ T_{21} &= \big[m - \Omega P_0\big(n_{\rm SS} + 2n_{\rm SS4}P_0 + 3n_{\rm SS6}P_0^2 + in_{\rm sFS} \\ &\quad + 2in_{\rm SFS4}P_0 + 3in_{\rm SFS6}P_0^2\big)\big], \\ T_{22} &= \big[k_2\Omega^2 - k_3\Omega^3 + ka_4\Omega^4 - k_5\Omega^5 + k_6\Omega^6 + m \\ &\quad - \Omega P_0\big(2n_{\rm SS} + 3n_{\rm SS4}P_0 + 4n_{\rm SS6}P_0^2 \\ &\quad + in_{\rm SFS} + 2in_{\rm SFS4}P_0 + 3in_{\rm SFS6}P_0^2\big)\big]. \end{aligned} \tag{14}$$

In order to find the MI gain, we should keep in mind that the wave number K of the perturbation can be found as the eigenvalue of the matrix $\left(\begin{smallmatrix} T_{11} & T_{12} \\ T_{21} & T_{22}\end{smallmatrix}\right)$, through the characteristic equation $\mathrm{Det}|T - KI| = 0$ with I being a 2×2 identity matrix. This leads to the dispersion relation

$$K = \tfrac{1}{2}[T_{11} + T_{22} + \sqrt{(T_{11} - T_{22})^2 + 4T_{12}T_{21}}]. \tag{15}$$

For MI to take place, the wave number K should get a nonzero imaginary part that will be responsible for an exponential growth of the perturbed amplitude. In general, the occurrence of MI is predicted through the power gain, defined as $G(\Omega) = 2\,\mathrm{Im}(K)$, which is obtained in this particular case in the form

$$G(\Omega) = \sqrt{\begin{matrix} c_2\Omega^2 - c_3\Omega^3 + c_4\Omega^4 - c_5\Omega^5 + c_6\Omega^6 \\ - c_7\Omega^7 + c_8\Omega^8 + c_{10}\Omega^{10} + c_{12}\Omega^{12}\end{matrix}}, \tag{16}$$

where

$$\begin{aligned} c_2 &= \big(8n_{\rm NL}P_0 + 16n_{\rm NL4}P_0^2 + 24n_{\rm NL6}P_0^3\big)k_2 \\ &\quad + 4n_{\rm SS}^2P_0^2 + 16n_{\rm SS4}n_{\rm SS}P_0^3 + 24n_{\rm SS}n_{\rm SS6}P^4 \\ &\quad + 16n_{\rm SS4}^2P_0^4 + 48n_{\rm SS4}n_{\rm SS6}P_0^5 + 36n_{\rm SS6}^2P_0^6 \\ &\quad + (8in_{\rm SFS}P_0 + 16in_{\rm SFS4}P_0^2 + 24in_{\rm SFS6}P_0^3 + 4) \\ &\quad \times \big(n_{\rm SS}P_0 + 2n_{\rm SS4}P_0^2 + 3n_{\rm SS6}P^3\big), \\ c_3 &= 8ik_2\big(n_{\rm SFS}P_0 + 2n_{\rm SFS4}P_0^2 + 3n_{\rm SFS6}P_0^3\big), \\ c_4 &= k_4\big(8n_{\rm NL}P_0 + 16n_{\rm NL4}P_0^2 + 24n_{\rm NL6}P_0^3\big) + 4k_2^2, \\ c_5 &= 8ik_4\big(n_{\rm SFS}P_0 + 2n_{\rm SFS4}P_0^2 + 3n_{\rm SFS6}P_0^3\big), \\ c_6 &= k_6\big(8n_{\rm NL}P_0 + 16n_{\rm NL4}P_0^2 + 24n_{\rm NL6}P_0^3\big) + 8k_2k_4, \\ c_7 &= 8ik_6\big(n_{\rm SFS}P_0 + 2n_{\rm SFS4}P_0^2 + 3n_{\rm SFS6}P_0^3\big), \\ c_8 &= 4k_4^2 + 8k_2k_6, \quad c_{10} = 8k_4k_6, \quad c_{12} = 4k_6^2. \end{aligned} \tag{17}$$

As it can be noted, the expression of the MI gain depends on many physical parameters. Considering all such parameters will make our contribution interesting but too heavy. Therefore, a suitable choice of parameters can be made based on previous works relative to the higher-order effect on soliton stability and the MI process. Originally, the terminology soliton was reserved for a particular set of integrable solutions existing due to the suitable balance between dispersion (or diffraction) and nonlinearity. Optical solitons are used for long- and short-distance information transmission. Unlike pulses in a linear dispersive fiber, solitons are self-confined, propagating long distances without changing shape. A well-known example of an equation that admits pulselike soliton solutions is the NLS equation. It is now well known that the power is directly proportional to the dispersion in the experimental investigation of optical solitons. Because of the large dispersion of the conventional single-mode fiber at the wavelength of minimal losses ($\lambda = 1.5\ \mu$m), a clear idea for power reduction was a shift of the operational wavelength towards the zero-dispersion wavelength [69–71] which is $\lambda = 1.31\ \mu$m. In doing so, an additional term in expanding the wave number of the fiber mode around the central frequency ω_0, namely, the TOD term, needs to be taken into account when extending the applicability of the NLS equation. Hence, there was a certain interest in understanding the effect of TOD on the existence and stability of the soliton [72–77] based on the Sasa-Satsuma [78] and Hirota [79] equations, which are the NLS equation with some TOD terms that cause great variation in MI properties which would induce some new nonlinear excitations. The linearized stability analysis for the Sasa-Satsuma equation [80] suggested that there are both MI and stability regimes for low perturbation frequencies on the continuous wave background. Indeed, it is well known that odd-order dispersion coefficients, such as TOD, do not affect

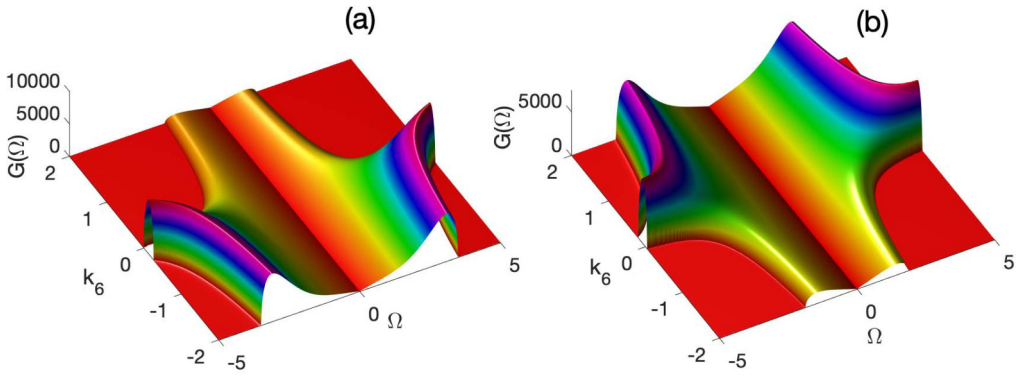

FIG. 1. The panels show plot of the variation of maximum MI gain as a function of perturbation frequency Ω and the SOD term k_6 for (a) the normal ($k_2 = 1$) and (b) the anomalous regimes ($k_2 = -1$) with the other parameters being: $P_0 = 8$, $k_5 = 0.00123$, $k_3 = 0.009$, $n_{\rm NL} = 1$, $n_{\rm NL4} = 1$, $n_{\rm NL6} = 0.03$, $n_{\rm SS} = -0.0247$, $n_{\rm SS4} = 0.037\,05$, $n_{\rm SS6} = -0.0247$, $n_{\rm SFS} = -0.030\,875$, $n_{\rm SFS4} = 0.0004$ and $n_{\rm SFS6} = 0.021$.

the MI condition [56]. The MI process has been revisited theoretically using a global stability analysis reformulated as an initial value problem. It has been demonstrated that MI gain of time-localized signals (i.e., pulsed signals) depends strongly on the TOD, leading to a dramatic reduction of the MI gain, contrary to the well-known case of time-extended signals (cw signals) [81]. The MI has been investigated in the region of minimum group-velocity dispersion through an extended NLS equation, taking into account FOD effects, and this term dominates the critical modulation-instability frequency when second-order dispersion approaches its minimum value at the so-called zero-dispersion wavelength [82]. The effect of TOD and FOD terms on MI has been investigated. It has been shown that the modulationally unstable waves evolve to the soliton-type characterized by the periodic generation of moving or stationary solitons and to a turbulent state, depending on the strength of the third- and fourth-order dispersion terms, which are related to the stability conditions for solitons [83]. It has been demonstrated numerically that in the presence of the quintic nonlinear term, which balances with the higher-order dispersion terms, the turbulent states can be controlled, leading to the periodic occurrence of the stable solitonlike pulses produced by MI of an extended NLS equation with the third- and fourth-order dispersion and the cubic-quintic nonlinear terms. It appears that even though the TOD term does not directly contribute to the MI gain spectrum, it influences the evolution of MI and the dynamics of the soliton [66]. Also, for a fiber with the zero group-velocity dispersion wavelength in the visible region of the spectrum and a pump wavelength close to the zero group-velocity dispersion wavelength, the importance of the FOD term in the expansion of the propagation constant is considerable, leading to a strong parametric gain of the sidebands even when technically the fiber is being pumped in the normal dispersion regime [34]. The FOD-induced MI, which can be used for broadband wavelength conversion, has been investigated experimentally in single-mode optical fiber, and evidence of a new MI spectral window due to the FOD effect in the normal-dispersion regime has been demonstrated [84]. MI of the HNLS equation with non-Kerr nonlinearities in an optical context has been studied, and an analytical expression for MI gain presented to show the effects of non-Kerr nonlinearities and higher-order dispersions on MI gain spectra [65]. The HNLS equation contains real parameters related to GVD, TOD, and FOD, SPM due to the cubic nonlinearity (Kerr effect), self-steepening, and self-frequency shift due to stimulated Raman scattering, and quintic non-Kerr nonlinearity, respectively. In particular, MI gain spectra for the cubic-quintic NLS equation with FOD and stimulated Raman scattering terms have been plotted. Indeed, the expression of the MI gain has revealed that the TOD

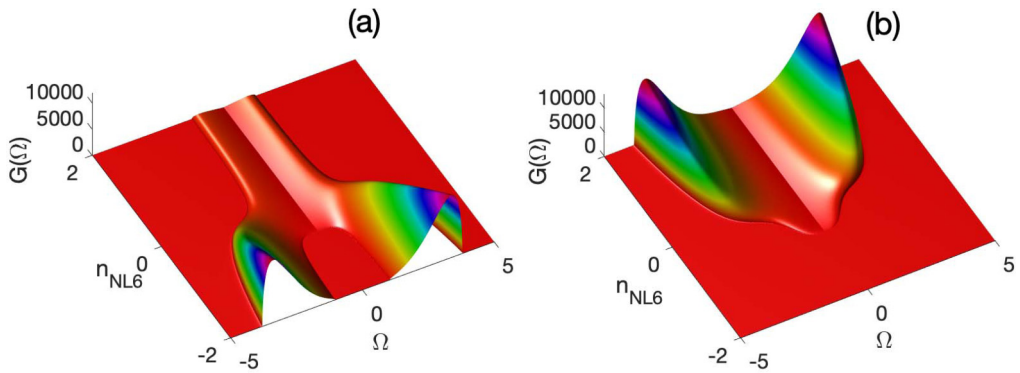

FIG. 2. The variation of maximum MI gain as a function of perturbation frequency Ω and the septic non-Kerr nonlinearity parameter $n_{\rm NL6}$. Panel (a) shows results for $k_6 = 0.02$, and panel (b) is plotted for $k_6 = -0.02$ with the other parameters being: $P_0 = 10$, $k_5 = 0.001\,23$, $k_3 = 0.009$, $n_{\rm NL} = 1$, $n_{\rm NL4} = 1$, $n_{\rm SS} = -0.0247$, $n_{\rm SS4} = 0.037\,05$, $n_{\rm SS6} = -0.0247$, $n_{\rm SFS} = -0.030\,875$, $n_{\rm SFS4} = 0.0004$, and $n_{\rm SFS6} = 0.021$.

term has no effect on the MI condition, but GVD and FOD terms influence the MI condition. The study also shows that the non-Kerr quintic nonlinear effect reduces the maximum value of the gain and bandwidth [65]. The MI process in glass fibers with a local saturable nonlinear refractive index, in operating conditions of anomalous dispersion but with a positive sign of the FOD, has been analyzed. It has been found that two types of MI processes become highly sensitive to the magnitude of the FOD. The first type of MI generates a single pair of sidebands, whereas the second type generates two pairs of sidebands [85]. However, among all the studies of the MI process in nonlinear optics, the question of MI analysis under the combined effects of higher-order dispersions, self-steepening, and self-frequency shift, cubic, quintic, and septic nonlinearities is investigated, here. That is why, in this paper, in particular, we insist on the balance between the sixth-order dispersion and nonlinearity terms on one hand, and between septic self-steepening and the septic self-frequency shift terms, on the other hand. To start, the gain spectrum is displayed in Fig. 1 versus the perturbation frequency Ω and the SOD parameter k_6 both for the normal [see Fig. 1(a)] and anomalous [see Fig. 1(b)] GVD regimes. For $k_2 > 0$, one notes two gain peaks that divert from the center $\Omega = 0$ when k_6 approaches zero. However, two regimes are detected, i.e., when $k_6 > 0$ lobes of the frequency domain are large and reduced for $k_6 < 0$, expanding the stability zone. The reverse scenario is obtained for $k_2 < 0$ where the large frequency bandwidth is observed for $k_6 > 0$ and small bandwidth is observed for $k_6 < 0$. In the rest of the stability analysis, the effects of higher-order nonlinear terms will be confronted to the two SOD regimes, i.e., $k_6 > 0$ and $k_6 < 0$ under normal GVD. The first example to be addressed in this regard is the impact of the nonlinear septic term on MI, which is depicted in Fig. 2 where panel (a) is plotted for $k_6 > 0$ and panel (b) for $k_6 < 0$. For the case $k_6 > 0$, high-intensity sidelobes appear for $n_{\mathrm{NL6}} < 0$, but the maximum gain increases, along with the frequency bandwidth, in the interval $-2 \leqslant n_{\mathrm{NL6}} < 0$. In this particular case, the bandwidth for $n_{\mathrm{NL6}} < 0$ is large and completely disappears for $n_{\mathrm{NL6}} \geqslant 0$, leaving two symmetric lobes of minor intensity but still enough for the cw to disintegrate into nonlinear structures. On the other side, when $k_6 < 0$, the instability is expected to be more pronounced for $n_{\mathrm{NL6}} > 0$ since the gain sidelobes are of high intensity and tend to disappear when $n_{\mathrm{NL6}} < 0$, although there is a low-intensity tongue of instability surrounded by a large region of stability [see Fig. 2(b)].

Figure 3 portrays the MI gain as a function of the quintic SS parameters and the frequency Ω for $k_4 > 0$ [panels (a) and (b)] and $k_4 < 0$ [panels (c) and (d)]. Each of the cases presents lobes of instability for normal and anomalous dispersion. In Fig. 3(a), for example, for which $k_2 > 0$, there appear two peaks of instability in the gain spectrum, which show instability to be possible for all values of n_{ss4}. The lobes being symmetric, the gap between them increases for $k_2 < 0$, and the instability bandwidth shrinks [see Fig. 3(b)]. The same spectrum of behaviors appears in Figs. 3(c) and 3(d) for which $k_4 < 0$. For $k_2 > 0$, the two symmetric lobes appear and get shrinked when $k_2 < 0$ for which there appears two breasts of instability. Also, the band gap between gain peaks has reduced. We should stress that the case $k_4 < 0$ and k_2 being

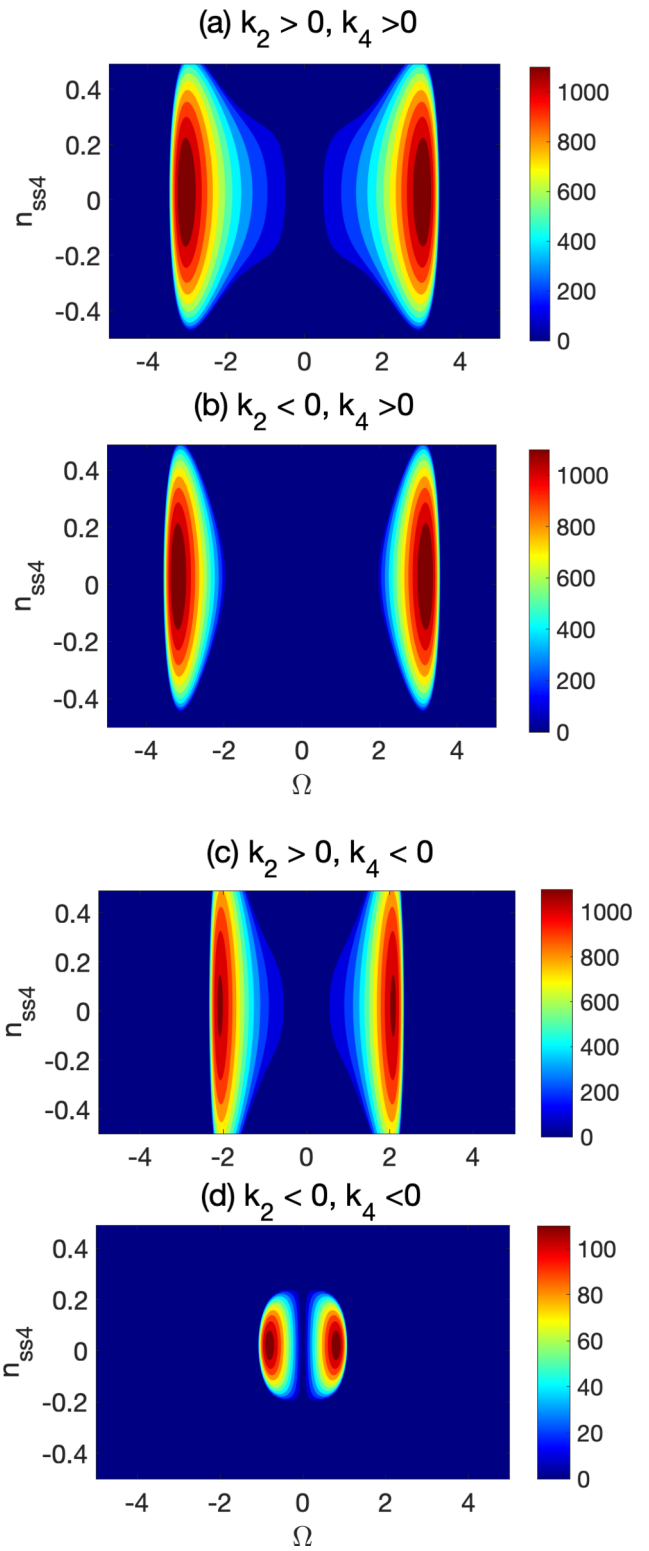

FIG. 3. Variation of maximum MI gain versus the perturbation frequency Ω and the quintic self-steepening term n_{SS4}. The FOD is considered positive in panels (a) and (b), respectively, obtained for $k_2 > 0$ and $k_2 < 0$. Panels (c) and (d) are plotted for a negative FOD coefficient k_4 with $k_2 > 0$ and $k_2 < 0$, respectively. The other parameters being: $P_0 = 10$, $k_6 = 0.02$, $k_5 = 0.001\,23$, $k_3 = 0.009$, $n_{\mathrm{NL}} = 1$, $n_{\mathrm{NL4}} = 1$, $n_{\mathrm{NL6}} = 0.03$, $n_{\mathrm{SS}} = -0.0247$, $n_{\mathrm{SS4}} = 0.037\,05$, $n_{\mathrm{SFS}} = -0.030\,875$, $n_{\mathrm{SFS4}} = 0.0004$, and $n_{\mathrm{SFS6}} = 0.021$.

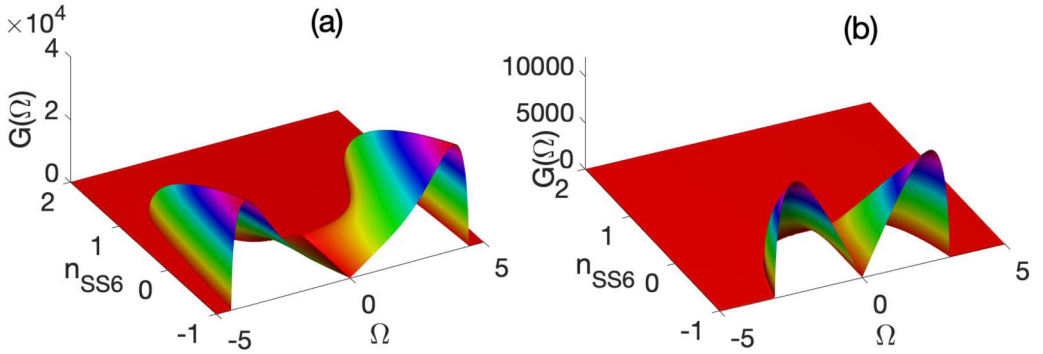

FIG. 4. Panels show the variation of maximum MI gain versus the perturbation frequency Ω and the septic self-steepening term n_{SS6} and for (a) $k_6 = 0.02$, (b) $k_6 = -0.02$ with the other parameters being: $P_0 = 10$, $k_5 = 0.001\,23$, $k_3 = 0.009$, $n_{NL} = 1$, $n_{NL4} = 1$, $n_{NL6} = 0.03$, $n_{SS} = -0.0247$, $n_{SS4} = 0.037\,05$, $n_{SFS} = -0.030\,875$, $n_{SFS4} = 0.0004$, and $n_{SFS6} = 0.021$.

either negative or positive were recently explored by Tiam *et al.* [86], who further found the existence of single-hump solitons numerically for positive values of $k_2 > 0$.

The competition between the septic SS and the SOD parameters is summarized in Fig. 4 where panels (a) and (b) correspond, respectively, to $k_6 > 0$ and $k_6 < 0$. In Fig. 4(a), when $k_6 > 0$, the MI gain is limited as n_{SS6} tends to zero and disappears at $n_{SS6} = 1$, leaving small intensity lobes separated by a large band gap frequency compared to the large frequency bandwidth observed for $-1 \leqslant n_{SS6} \leqslant 0$. For the case $k_6 < 0$ [see Fig. 4(b)], no instability should be expected for $n_{SS6} > 0$. However, two symmetric lobes show the presence of instability under a suitable balance between nonlinear and dispersive effects. The MI gain as a function of the perturbation frequency Ω and the SFS parameter is plotted in Fig. 5 with panels (a) and (b), respectively, corresponding to $k_6 > 0$ and $k_6 < 0$. In general, two distinct and symmetric sidebands appear in the gain spectrum and remain the same even with increasing n_{SFS6}. However, the bandwidth is larger for $k_6 < 0$ than when k_6 is positive. From the expression of the gain (16), the reader may note that the odd terms of coefficients k_3 and k_5 do not contribute to the dynamics of the MI growth rate. This is a confirmation of predictions from Shagalov [83] who proposed a separated technique to study the impact of such terms in the numerical occurrence of MI. In so doing, the relationship between soliton emergence and MI has been debated in several contributions. Especially, attention has been paid to the stability of solitons as they share the same parameter conditions with the occurrence of MI. Before proceeding to the numerical analysis of our above predictions, it would be of interest to investigate the impact of each of the parameters and their various combinations for the emergence and stability of solitons.

B. Stability of solitons and MI occurrence

When $k_2 \neq 0$, $n_{NL} \neq 0$ with the rest of the coefficients being equal to zero, we are in the presence of the cubic quintic NLS equation that admits stable soliton solutions. Such solutions imply the appearance of MI and the subsequent appearance of wave trains under the condition that dispersion and nonlinearity be well balanced. However, when the high-dispersion terms are different from zero, the stability of soliton solution gets alternated with a substantial impact on the appearance of MI, primarily when the long-time evolution of solitary waves is investigated. Therefore, before proceeding to the numerical analysis of MI, it is necessary to examine the impact of each dispersion term and their combinations on the emergence of stable solitons in the model under study. To investigate the effects of such parameters on soliton stability, we adopt the method developed in Ref. [76] and recently used by Shagalov [83].

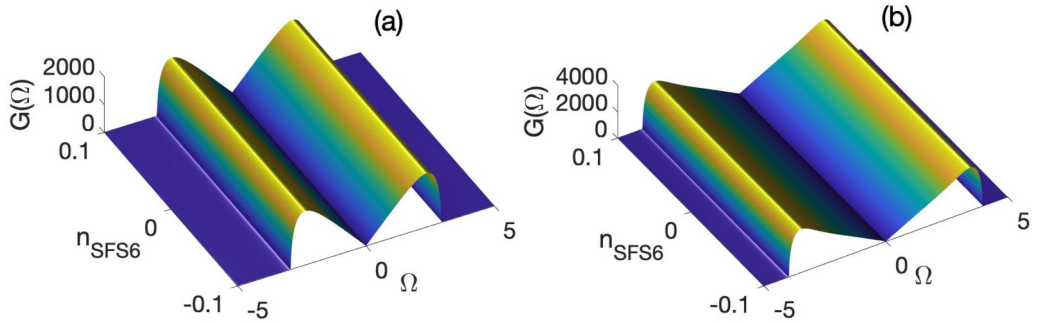

FIG. 5. Variation of maximum MI gain versus the perturbation frequency Ω and the septic self-frequency shift term n_{SFS6} and for (a) $k_6 = 0.02$, (b) $k_6 = -0.02$ with the other parameters being: $P_0 = 10$, $k_5 = 0.001\,23$, $k_3 = 0.009$, $n_{NL} = 1$, $n_{NL4} = 1$, $n_{NL6} = 0.03$, $n_{SS} = -0.0247$, $n_{SS4} = 0.037\,05$, $n_{vSS6} = -0.0247$, $n_{SFS} = -0.030\,875$, and $n_{SFS4} = 0.0004$.

A small-amplitude wave $u(Z,\tau) = u_0 e^{-ikZ+i\omega\tau}$ is adopted as a trial solution to Eq. (7), which leads to the dispersion relation,

$$k(\omega) = -k_2\omega^2 + k_3\omega^3 - k_4\omega^4 + k^5\omega^5 - k_6\omega^6. \tag{18}$$

To proceed, we focus on the zero-dispersion regime, which implies the relation $\frac{k(\omega)}{\omega} = 0$ whose real solutions imply a resonance interaction between the soliton and the small-amplitude wave leading to a stable soliton solution. This depends on a number of combinations between the dispersion coefficients k_2, k_3, k_4, k_5, and k_6. With no pretension of being exhaustive, we focus mainly on the following cases:

(i) For $k_4 = k_5 = k_6 = 0$, $k_2 \neq 0$, and $k_3 \neq 0$, Eq. (18) admits the solution $\omega_r = k_2/k_3$. The soliton may be unstable and its decay will take place with emission of waves with frequency ω_r under the condition $k_2 < 0$ and $k_3 > 0$ or $k_2 > 0$ and $k_3 < 0$. This particular case in commonly known and several numerical simulations have confirmed the results.

(ii) For $k_3 = k_5 = k_6 = 0$, $k_2 \neq 0$, and $k_4 \neq 0$, the dispersion relation will admit the solutions $\omega_r = \pm\sqrt{-k_2/k_4}$, which implies that the soliton will be stable if $k_2/k_4 >$ and unstable if $k_2/k_4 < 0$.

(iii) For $k_3 \neq 0$, $k_5 = k_6 = 0$, $k_2 \neq 0$, and $k_4 \neq 0$, two roots are obtained for the dispersion relation: $\omega = \frac{-k_3 \mp \sqrt{k_3^2 - 4k_2k_4}}{2k_4}$. Solutions will be two real roots for $k_3^2 - 4k_2k_4 > 0$, which leads to the condition $k_2k_4 > k_3^2/4$ for the soliton to be stable.

(iv) For $k_2 \neq 0$, $k_3 \neq 0$, $k_4 \neq 0$, $k_5 \neq 0$, and $k_6 = 0$, the dispersion relation reduces to a third-order polynomials and the stability of the soliton can be studied through the Routh-Hurwitz (RH) criterion. In doing so, the soliton will be stable so that MI takes place if the conditions $k_4/k_5 \leqslant 0$, $k_2/k_5 \leqslant 0$, and $k_4k_3 \geqslant k_2k_5$ are simultaneously satisfied.

(v) For $k_2 \neq 0$, $k_3 \neq 0$, $k_4 \neq 0$, $k_5 \neq 0$, and $k_6 \neq 0$, the RH stability criterion, from the obtained fourth-order polynomials, imposes $k_6 < 0$, $k_5 > 0$, $k_4 < 0$, $k_3 > 0$, $k_2 < 0$, $k_4k_5 > k3k_6$, and $k_3k_4k_5 > k_3^2k_6 + k_2k_5^2$ for the soliton to be stable.

(vi) For $k_2 \neq 0$, $k_3 \neq 0$, $k_4 \neq 0$, $k_5 = 0$, and $k_6 \neq 0$, from the RH stability criterion, we get $k_6 < 0$, $k_4 < 0$, $k_3 > 0$, $k_2 < 0$, and $k_3k_6 > 0$ for the soliton to be stable and MI to take place.

(vii) For $k_2 \neq 0$, $k_3 = 0$, $k_4 = 0$, $k_5 = 0$, and $k_6 = 0$, the dispersion relation (18) has the soliton $\omega_r = \sqrt[3]{k_2/k_5}$ so that for $k_2/k_5 > 0$, the soliton will be stable and unstable otherwise. In this particular case, it also obvious that the fifth-order nonlinearity stabilizes the soliton and gives more chances to the MI to take place.

The stability of solitons reveals more interesting and underlying phenomena that are mostly related to the appearance of wave trains via the activation of MI. This is true as it has long been proven that solitons and MI share the same parameter region. This gets more complicated when several parameters are involved and require more argument input to justify parameter values' choice and their contribution to the studied MI process. For instance, from the above analysis, we have realized that higher-order dispersion terms contribute to stabilizing the soliton and, therefore, play a vital role in the process of MI. However, the above stability analysis being local, addressing a more complete version of the study via a long-time numerical simulation of the predicted entities is necessary. This is for the simple reason that the model contains nonlinear and dispersive nonlinear terms beyond the dispersion terms, which may violate some of the above stability criteria and lead to new phenomena and behaviors in the long-time evolution of modulationally unstable wave patterns. This will somehow justify our choice of parameter values in the study of the MI gain and give more credit to the proposed model.

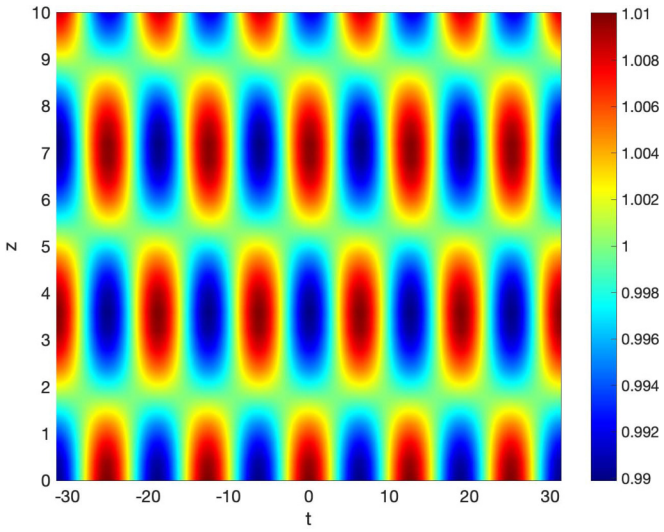

FIG. 6. The panels show the evolution of the cw under condition (vii) of the soliton stability analysis which predict MI to be violated if $k_2/k_5 < 0$ with $k_2 = -1$ and $k_5 = 0.001\,23$. The rest of the parameters are: $k_6 = 0$, $P_0 = 10$, $k_3 = 0$, $k_4 = 0$, $n_{\rm NL} = 1$, $n_{\rm NL4} = 1$, $n_{\rm NL6} = 0.03$, $n_{\rm SS} = -0.0247$, $n_{\rm SS4} = 0.037\,05$, $n_{\rm SS6} = -0.0247$, $n_{\rm SFS} = -0.030\,875$, $n_{\rm SFS4} = 0.0004$, and $n_{\rm SFS6} = 0.021$.

IV. NUMERICAL ANALYSIS OF UNSTABLE WAVE MODULATION

To check the accuracy of our linear stability analysis, direct numerical simulations have been performed on the model Eq. (7). Of course, a particular scenario of the MI development strongly depends on the type of initial conditions considered, namely, noisy perturbations of the plane wave, localized perturbations of the plane wave, and harmonic perturbations of the plane wave, respectively. In particular, a general solution of the equation governing the evolution of the spatiotemporal of MI perturbation in terms of a combination of cosine and sine hyperbolic functions has been obtained. In this paper, with the ambition to generate bright solitons via MI, the right perturbation to be adopted is a weak sine perturbation so that the initial condition be of the form [17]

$$u(0,t) = \sqrt{P_0}[1 + a_m \sin(\Omega_m t)]e^{i\phi_{\rm NL}}, \tag{19}$$

where $a_m = 0.01$ is the modulational amplitude and $\Omega_m = 0.5$ is the frequency of a weak sinusoidal modulation frequency imposed on the cw wave. The value of Ω_m is within the bandwidth that is supposed to give rise to unstable waves. Numerical results are obtained from Eq. (7) through the

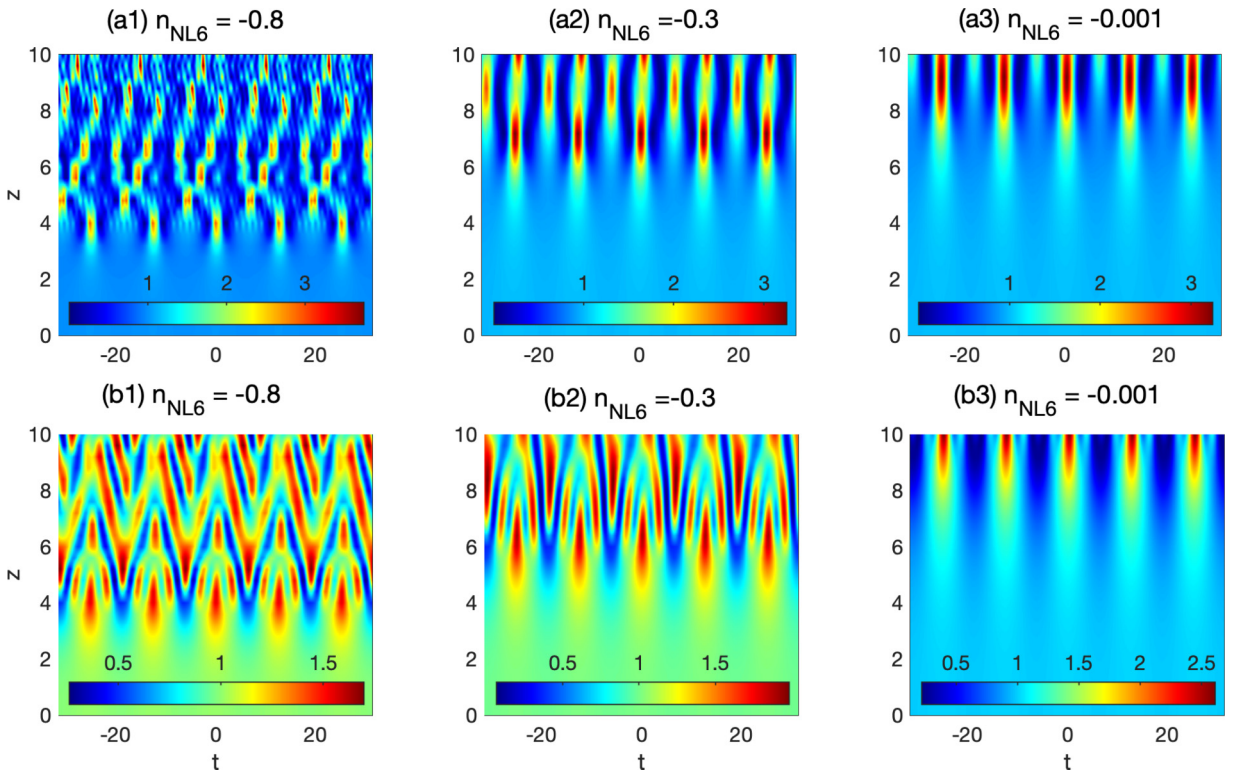

FIG. 7. The panels show the evolution of the cw under the effect of the septic nonlinearity term for $(\mathrm{aj})_{j=1-3}$ $k_6 = 0.0008$, $(\mathrm{bj})_{j=1-3}$ $k_6 = -0.0008$, and $P_0 = 10$, $k_5 = 0.001\,23$, $k_3 = 0.009$, $n_{\mathrm{NL}} = 1$, $n_{\mathrm{NL4}} = 1$, $n_{\mathrm{NL6}} = 0.03$, $n_{\mathrm{SS}} = -0.0247$, $n_{\mathrm{SS4}} = 0.03705$, $n_{\mathrm{SS6}} = -0.0247$, $n_{\mathrm{SFS}} = -0.030875$, $n_{\mathrm{SFS4}} = 0.0004$, and $n_{\mathrm{SFS6}} = 0.021$.

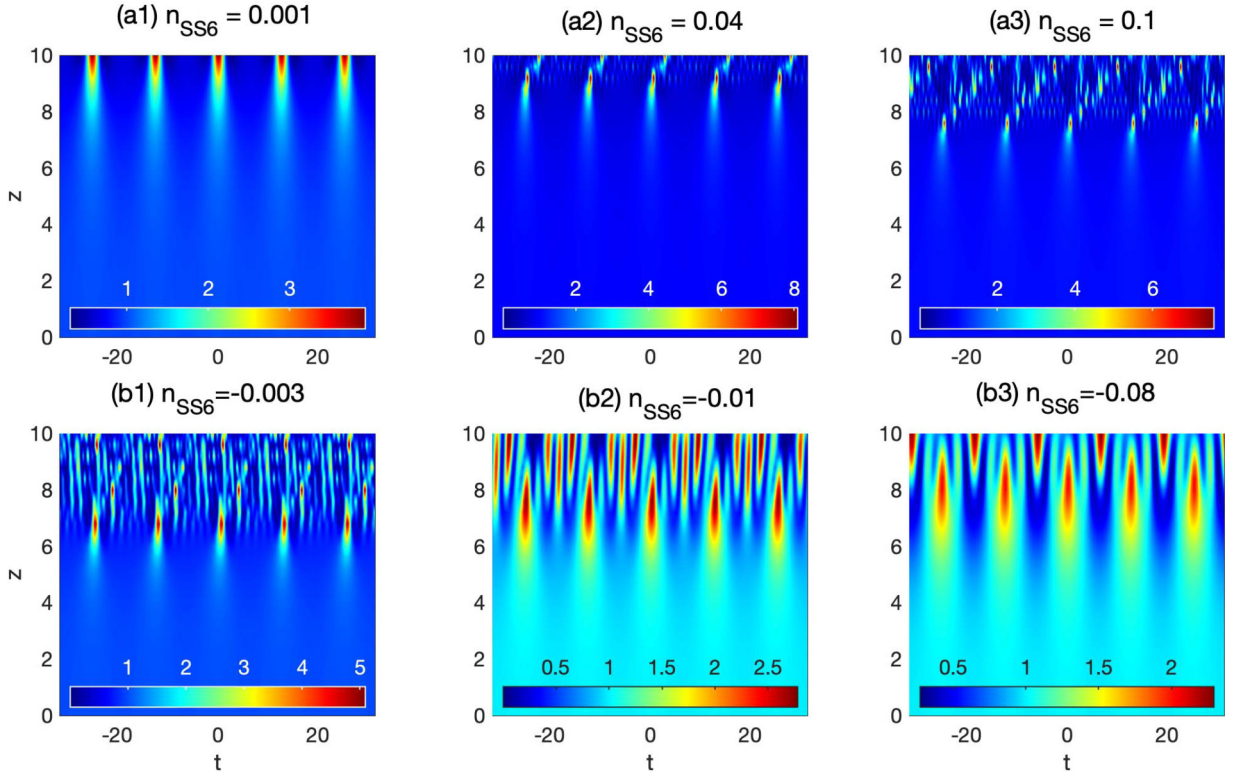

FIG. 8. The panels show the evolution of the cw under the effect of the septic self-steepening term for: $(\mathrm{aj})_{j=1-3}$ $k_6 = 0.0003$, $(\mathrm{bj})_{j=1-3}$ $k_6 = -0.0003$, and $P_0 = 10$, $k_5 = 0.001\,23$, $k_3 = 0.009$, $n_{\mathrm{NL}} = 1$, $n_{\mathrm{NL4}} = 1$, $n_{\mathrm{NL6}} = 0.03$, $n_{vSS} = -0.0247$, $n_{\mathrm{SS4}} = 0.037\,05$, $n_{\mathrm{SFS}} = -0.030\,875$, $n_{\mathrm{SFS4}} = 0.0004$, and $n_{\mathrm{SFS6}} = 0.021$.

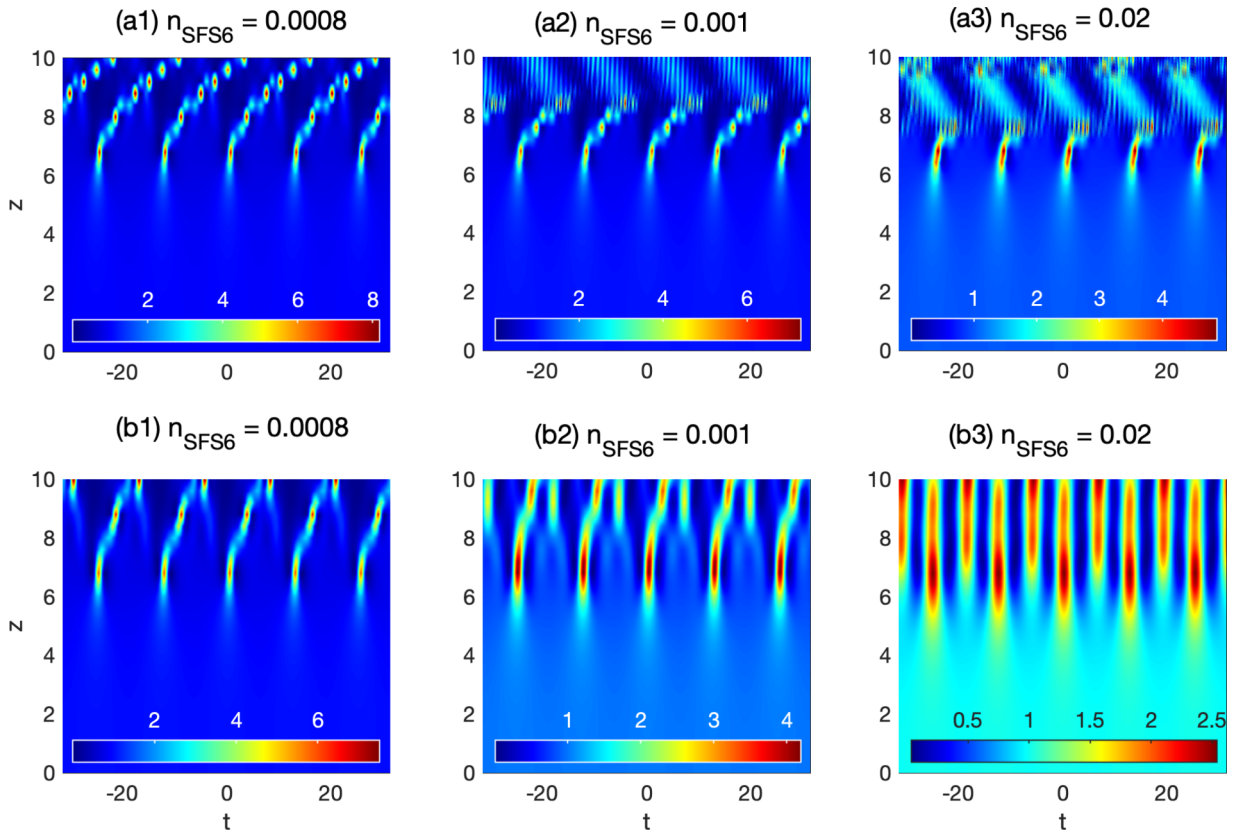

FIG. 9. The panels show the evolution of the cw under the effect of the septic self-frequency shift term for: $(\mathrm{aj})_{j=1-3}$ $k_6 = 0.0008$, $(\mathrm{bj})_{j=1-3}$ $k_6 = -0.0008$, and $P_0 = 10$, $k_5 = 0.001\,23$, $k_3 = 0.009$, $n_{\mathrm{NL}} = 1$, $n_{\mathrm{NL4}} = 1$, $n_{\mathrm{NL6}} = 0.03$, $n_{\mathrm{SS}} = -0.0247$, $n_{\mathrm{SS4}} = 0.037\,05$, $n_{\mathrm{SS6}} = -0.0247$, $n_{\mathrm{SFS}} = -0.030\,875$, and $n_{\mathrm{SFS4}} = 0.0004$.

split-step Fourier method with a particular interest in the emergence of MI as a result of the balanced competition among SOD and septic nonlinearity, self-steepening, and self-frequency shift effects. To start, it is of importance to confirm the stability of soliton performed in the previous section through one of the cases, (vii), for example. It is predicted that for $k_2/k_5 > 0$, the soliton solution will be stable, and MI will be likely to occur. Otherwise, the soliton solution will be unstable, taking away all chances for MI to emerge in the system. We deliberately violate the stability condition by imposing $k_2/k_5 < 0$, which leads to the patterns obtained in Fig. 6 where the cw breaks into wave patterns that have the shape of solitonic objects. This shows such conditions might be true, but they are balanced by the other parameters that may violate the soliton solution's stability condition. Otherwise, such conditions are not enough to predict instability, which justifies the results from different gain spectra where instability is possible negative and positive values of parameters. This explains why we insist on the competitive effect between higher-order nonlinearity and dispersion in the rest of the paper.

In Fig. 7, under normal GVD, results are presented for $k_6 > 0$ [see Fig. 7(aj)$_{j=1-3}$] and $k_6 < 0$ [see Fig. 7(bj)$_{j=1-3}$] with n_{NL6} changing in each of the cases. When $k_6 > 0$, the chosen values of parameters in gain spectra give rise to nonlinear patterns as predicted. Particularly, for $n_{\mathrm{NL6}} = -0.8$, the instability takes place early, but increasing the nonlinear septic parameter reduces the recurrence of the patterns which develop after a long distance. The same phenomenon is obvious when $k_6 < 0$, except that patterns appear to be exotic pulses whose frequency and recurrence change with the propagation distance. Remarkably, for higher values of n_{NL6} both for k_6 positive and negative, the perturbed cw breaks up into amplified pulses: The amplitude increases gradually during propagation. It is then ostensible that whereas controlling the occurrence of MI in the fiber through the septic nonlinearity, different scenarios, such as wave trains, erratic patterns of high or low amplitude can appear, depending on the competition among the various intrinsic nonlinearities and dispersions. Indeed, this could not be predicted via the linear stability analysis. Still, the obtained results reinforce the efficiency of the MI mechanism through which optical wave patterns of various forms and characteristics can be generated. This is more reinforced by the instability features obtained in Fig. 8, which picture the effect of the SS term on the long time evolution of the perturbed cw both for $k_6 > 0$ [see Fig. 8(aj)$_{j=1-3}$] and $k_6 < 0$ [see Fig. 8(bj)$_{j=1-3}$]. We should, however, stress here that given the spectrum of behaviors obtained from the gain of Fig. 4, the maximum gain is located in the region $n_{\mathrm{SS6}} < 0$ so that one expects the cw to disintegrate likely for such value. However, considering the case $k_6 > 0$, the panels $(\mathrm{aj})_{j=1-3}$ of Fig. 8 show that with increasing n_{SS6}, the MI patterns change from progressively amplified pulses to many erratic patterns with a tendency to shift on the right. On the other side, when we consider $k_6 < 0$, given that

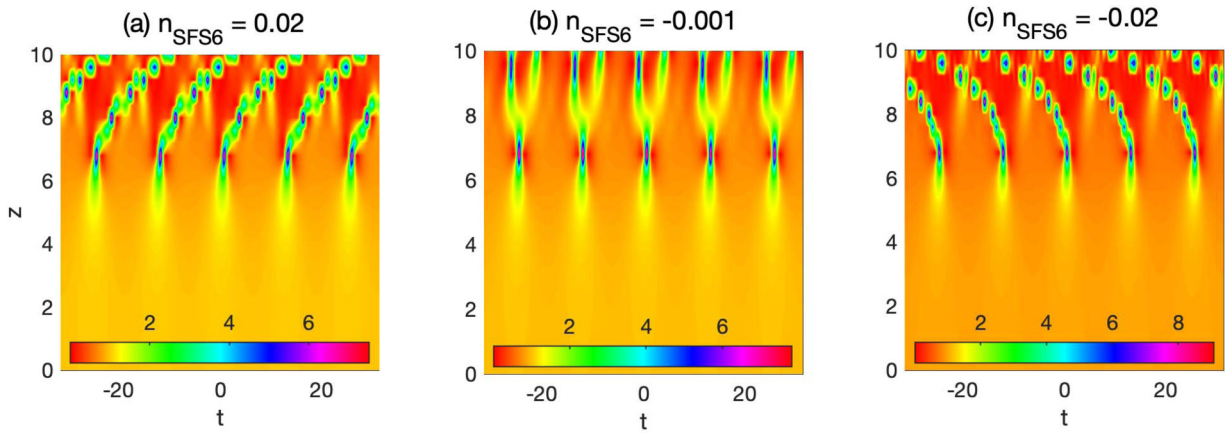

FIG. 10. Effect of the septic self-frequency shift term on the propagation direction of the disintegrated cw for (a) $n_{\mathrm{SFS6}} = 0.02$, $k_6 = 0.0008$, (b) $n_{\mathrm{SFS6}} = -0.001$, $k_6 = 0.0008$, (c) $n_{\mathrm{SFS6}} = -0.02$, $k_6 = -0.0008$, and $P_0 = 10$, $k_5 = 0.001\,23$, $k_3 = 0.009$, $n_{\mathrm{NL}} = 1$, $n_{\mathrm{NL4}} = 1$, $n_{\mathrm{NL6}} = 0.03$, $n_{\mathrm{SS}} = -0.0247$, $n_{\mathrm{SS4}} = 0.037\,05$, $n_{\mathrm{SS6}} = -0.0247$, $n_{\mathrm{SFS}} = -0.030\,875$, and $n_{\mathrm{SFS4}} = 0.0004$.

the MI bandwidth is exclusively situated in the area where $n_{\mathrm{SS6}} < 0$ is negative, decreasing its value produces the same effect except that for $n_{\mathrm{SS6}} = -0.01$ and $n_{\mathrm{SS6}} = -0.08$, the MI takes place in the form of alternating multihumped pulses. One fact that is, however, common in the theory of solitons is also obvious here, the space and time expansions of solitonic objects influences their characteristics, mainly the intensity for $n_{\mathrm{SS6}} = -0.003$, the light patterns are smaller with high intensity compared to the rest of the cases.

Figure 9 shows the behaviors of the unstable cw when the SFS changes both for k_6 positive and negative. Under the condition $k_6 > 0$, one sees from Fig. 9(a1) that for $n_{\mathrm{SFS6}} = 0.0008$, the long time evolution of MI is characterized by right-shifted patterns. With increasing the effect of the SFS, the shifted coherent optical patterns travel over a short distance and turn into erratic structures shifted toward the left [see Fig. 9(a2)]. This later feature gets pronounced when $n_{\mathrm{SFS6}} = 0.02$ where there is a mix up of coherent optical patterns along with left-shifted erratic modulated structures as shown in Fig. 9(a3). Under the same conditions as in Fig. 9(aj)$_{j=1-3}$ but with $k_6 < 0$, the optical patterns generated by MI are of low intensity [see Fig. 9(b1)], shifted to the right. However, the action of the increasing SFS effect reduces the number of wave trains, leaving patterns that are extended over the distance [see Fig. 9(b2)], which, for $n_{\mathrm{SFS6}} = 0.02$ turn out to be trains of alternating and oscillating pulses [see Fig. 9(b3)]. Indubitably, the direction of the propagating solitons is importantly affected by the septic SFS term, and such a direction can change when parameters are well balanced with appropriate signs. In the numerical experiment shown in Fig. 10, one clearly confirms that when n_{SFS6} and k_6 are positive, the solitonic patterns are shifted to the right [see Fig. 10(a)], which is corrected for $n_{\mathrm{SFS6}} = -0.001$ as seen in Fig. 10(b). Nevertheless, it is found that the direction can shift to the left for $n_{\mathrm{SFS6}} = -0.02$ and $k_6 < 0$. As said earlier, model Eq. (7) contains many parameters that render it difficult to control the dynamics of any emerging pattern. In the meantime, we should stress that studies have been carried out on earlier models in the absence of the higher-order dispersive and nonlinear effects, such as the septic nonlinearity, the septic self-steepening, and the self-phase shift terms.

V. CONCLUSION

In this paper, we have successfully derived a generalized higher-order NLS equation with cubic, quintic, and septic nonlinearity with self-steepening and self-frequency shift terms of the septic order. Under the linear stability analysis of a cw solution, an analytical expression for the MI gain has been derived, and its sensitivity to the competitive effects among the SOD, the septic nonlinearity, the self-steepening, and self-frequency shift terms have been addressed. Different combinations of the dispersion coefficients have been explored that give rise to soliton stability and the emergence of MI. It was revealed that the instability condition for the soliton could be violated due to the presence of higher-order nonlinear terms. This has been confirmed via direct numerical simulations where under various dispersive and nonlinear effects, the cw has been found to disintegrate into trains of structures with solitonic features. Interestingly, during numerical experiments, we have discovered that the propagation direction of the trains of waves can be controlled by a suitable balance between the SOD and the septic self-frequency shift strength. This may be a valuable tool with undeniable and straightforward applications in nonlinear optic communications.

ACKNOWLEDGMENTS

The work by C.B.T. was supported by the Botswana International University of Science and Technology under Grant No. DVC/RDI/2/1/16I (25). C.B.T. thanks the Kavli Institute for Theoretical Physics (KITP), University of California Santa Barbara (USA).

APPENDIX: PARAMETERS FOR EQ. (6)

Parameters for Eq. (6) are defined as follows:

$$\beta_m = \frac{1}{m!}\left(\frac{\partial^m \beta}{\partial \omega^m}\right)_0, \quad (m = 2\text{–}6), \quad \gamma_1 = \left(\frac{\partial \beta}{\partial |\psi|^2}\right)_0 + \frac{k_0 n_2}{4A_{\mathrm{eff}}},$$

$$\gamma_2 = \frac{1}{2}\left(\frac{\partial \beta}{\partial |\psi|^4}\right)_0 + \frac{k_0}{16A_{\mathrm{eff}\,1}}\left(\frac{n_2^2}{2} + n_4\right),$$

$$\gamma_3 = \frac{1}{6}\left(\frac{\partial\beta}{\partial|\psi|^6}\right)_0 + \frac{k_0}{64A_{\text{eff}\,2}}\left(n_6 + \frac{n_4 n_2}{n(\omega)}\right), \qquad \alpha_4 = \frac{1}{2}\left(\frac{\partial\beta}{\partial(|\psi|^4)_t}\right)_0, \quad \alpha_6 = \frac{1}{6}\left(\frac{\partial\beta}{\partial(|\psi|^6)_t}\right)_0,$$

$$\alpha_1 = \left(\frac{\partial^2\beta}{\partial\omega\,\partial(|\psi|^2)}\right)_0, \quad \alpha_3 = \frac{1}{2}\left(\frac{\partial^2\beta}{\partial\omega\,\partial(|\psi|^4)}\right)_0, \qquad \text{(A1)}$$

$$\alpha_5 = \frac{1}{6}\left(\frac{\partial^2\beta}{\partial\omega\,\partial(|\psi|^6)}\right)_0, \quad \alpha_2 = \left(\frac{\partial\beta}{\partial(|\psi|^2)_t}\right)_0,$$

where $A_{\text{eff}} = \frac{\int_{-\infty}^{\infty}\int_{-\infty}^{\infty}|F(x,y)|^2dx\,dy}{\int_{-\infty}^{\infty}\int_{-\infty}^{\infty}|F(x,y)|^4dx\,dy}$, $A_{\text{eff}\,1} = \frac{\int_{-\infty}^{\infty}\int_{-\infty}^{\infty}|F(x,y)|^2dx\,dy}{\int_{-\infty}^{\infty}\int_{-\infty}^{\infty}|F(x,y)|^6dx\,dy}$, $A_{\text{eff}\,2} = \frac{\int_{-\infty}^{\infty}\int_{-\infty}^{\infty}|F(x,y)|^2dx\,dy}{\int_{-\infty}^{\infty}\int_{-\infty}^{\infty}|F(x,y)|^8dx\,dy}$ with A_{eff} as the refractive core area of the fiber. $A_{\text{eff}\,1} = (3/4)A_{\text{eff}}$ and $A_{\text{eff}\,1} = (1/2)A_{\text{eff}}$.

[1] G. B. Whitham, Proc. R. Soc. London, Ser. A **283**, 238 (1965).
[2] T. B. Benjamin and J. E. Feir, J. Fluid Mech. **27**, 417 (1967).
[3] V. I. Karpman, JETP Lett. **6**, 277 (1967).
[4] G. P. Agrawal, *Nonlinear Fiber Optics*, 5th ed. (Academic, New York, 2013).
[5] A. R. Seadawy and D. Lu, Results Phys. **7**, 43 (2017).
[6] A. Mahalingam and K. Porsezian, Phys. Rev. E **64**, 046608 (2001).
[7] R. Yang, R. Hao, L. Li, Z. Li, and G. Zhou, Opt. Commun. **242**, 285 (2004).
[8] A. Hasegawa and F. Tappert, Appl. Phys. Lett. **23**, 142 (1973).
[9] A. Hasegawa and F. Tappert, Appl. Phys. Lett. **23**, 171 (1973).
[10] L. F. Mollenauer, R. H. Stolen, and J. P. Gordon, Phys. Rev. Lett. **45**, 1095 (1980).
[11] L. F. Mollenauer. R. H. Stolen, J. P. Gordon, and W. J. Tomlinson, Opt. Lett. **8**, 289 (1983).
[12] H. Takara, T. Ohara, K. Mori, K. Sato, E. Yamada, Y. Inoue, T. Shibata, M. Abe, T. Morioka, and K.-I. Sato, Electron. Lett. **36**, 2089 (2000).
[13] M. Nisoli, S. De Silvestri, O. Svelto, R. Szipöcs, K. Ferencz, C. Spielmann, S. Sartania, and F. Krausz, Opt. Lett. **22**, 522 (1997).
[14] T. Hori, N. Nishizawa, T. Goto, and M. Yoshida, J. Opt. Soc. Am. B **21**, 1969 (2004).
[15] A. Hasegawa and Y. Kodama, *Solitons in Optical Communications* (Clarendon, Oxford, 1995).
[16] M. J. Ablowitz, *Solitons, Nonlinear Evolution Equations and Inverse Scattering* (Cambridge University Press, Cambridge, U.K., 1992).
[17] G. P. Agrawal, *Nonlinear Fiber Optics*, 3rd ed. (Academic, San Diego, 2001).
[18] A. I. Maimistov and A. M. Basharov, *Nonlinear Optical Waves* (Springer, Berlin, 1999).
[19] C. Liu, Z. Y. Yang, L. C. Zhao, and W. L. Yang, Phys. Rev. E **91**, 022904 (2015).
[20] C. Liu, Z. Y. Yang, L. C. Zhao, L. Duan, G. Yang, and W. L. Yang, Phys. Rev. E **94**, 042221 (2016).
[21] X. Gao, Appl. Math. Lett. **73**, 143 (2017).
[22] L. Liu, and B. Tian, H. P. Chai, and Y. Q. Yuan, Phys. Rev. E **95**, 032202 (2017).
[23] M. Gedalin, T. C. Scott, and Y. B. Band, Phys. Rev. Lett. **78**, 448 (1997).
[24] M. J. Ablowitz, B. Prinari, and A. D. Trubatch, *Discrete and Continuous Nonlinear Schrödinger Systems* (Cambridge University Press, Cambridge, U.K., 2003).
[25] C. J. Chen, P. K. A. Wai, and C. R. Menyuk, Opt. Lett. **19**, 198 (1994).
[26] C. J. Chen, P. K. A. Wai, and C. R. Menyuk, Opt. Lett. **20**, 350 (1995).
[27] Y. Kodama and A. Hasegawa, IEEE J. Quantum Electron. **23**, 510 (1987).
[28] Z. Li, L. Li, H. Tian, and G. Zhou, Phys. Rev. Lett. **84**, 4096 (2000).
[29] J. Tian, H. Tian, Z. Li, L. Kang, and G. Zhou, Phys. Scr. **67**, 325 (2003).
[30] J. M. Soto-Crespo and L. Pesquera, Phys. Rev. E **56**, 7288 (1997).
[31] Y. Xiao, B. Xiaoqin, and L. Tingting, Optik **186**, 315 (2019).
[32] T. Taniuti and H. Washimi, Phys. Rev. Lett. **21**, 209 (1968).
[33] G. P. Agrawal, *Nonlinear Fiber Optics, Optics and Photonics*, 4th ed. (Academic, New York, 2009).
[34] J. D. Harvey, R. Leonhardt, S. Coen, G. Wong, J. Knight, W. J. Wadsworth, and P. St. J. Russell, Opt. Lett. **28**, 2225 (2003).
[35] Y. Kivshar and G. P. Agrawal, *Optical Solitons: From Fibers to Photonic Crystals*, 1st ed. (Academic, San Diego, 2003).
[36] R. Ganapathy and V. C. Kuriakose, Pramana J. Phys. **58**, 669 (2002).
[37] S. Sudo, H. Itoh, K. Okamoto, and K. Kubodera, Appl. Phys. Lett. **54**, 993 (1989).
[38] R. V. J. Raja, K. Porsezian, and K. Nithyanandan, Phys. Rev. A **82**, 013825 (2010).
[39] J. M. Chvez Boggio, S. Tenenbaum, and H. L. Fragnito, J. Opt. Soc. Am. B **18**, 1428 (2001).
[40] S. Liu, Appl. Phys. Lett. **89**, 171118 (2006).
[41] C. Martijn de Sterke, J. Opt. Soc. Am. B **15**, 2660 (1998).
[42] C. R. Phillips and M. M. Fejer, J. Opt. Soc. Am. B **27**, 2687 (2010).
[43] H. Ward, M. N. Ouarzazi, M. Taki, and P. Glorieux, Eur. Phys. J. D. **3**, 275 (1998).
[44] A. Mohamadou, B. E. Ayissi, and T. C. Kofané, Phys. Rev. E **74**, 046604 (2006).
[45] F. II Ndzana, A. Mohamadou, and T. C. Kofané, Opt. Commun. **275**, 421 (2007).
[46] C. G. Latchio Tiofack, A. Mohamadou, T. C. Kofané, and A. B. Moubissi, Phys. Rev. E **80**, 066604 (2009).
[47] C. M. Ngabireng, S. Ambomo, P. T. Dinda, and A. B. Moubissi, J. Opt. **13**, 085201 (2011).
[48] L. M. Mandeng and C. Tchawoua, J. Opt. Soc. Am. B **30**, 1382 (2013).
[49] X. Zhong, X. Du, and K. Cheng, Opt. Express **23**, 29467 (2015).
[50] A. Blanco-Redondo, C. M. de Sterke, J. E. Sipe, T. F. Krauss, B. J. Eggleton, and C. Husko, Nat. Commun. **7**, 10427 (2016).
[51] J. C. Knight, T. A. Birks, J. C. Knights, and P. St. J. Russell, Opt. Lett. **21**, 1547 (1996).
[52] P. St. J. Russell, Science **299**, 358 (2003).

[53] B. J. Eggleton, C. Kerbage, P. Westbrook, R. S. Windeler, and A. Hale, Opt. Express **9**, 698 (2001).
[54] J. H. Lee, Z. Yusoff, W. Belardi, M. Ibsen, T. M. Monro, and D. J. Richardson, Opt. Lett. **27**, 927 (2002).
[55] F. Biancalana, D. V. Skryabin, and P. St. J. Russell, Phys. Rev. E **68**, 046603 (2003).
[56] M. J. Potasek, Opt. Lett. **12**, 921 (1987).
[57] K. J. Blow and D. Wood, IEEE J. Quantum Electron. **25**, 2665 (1989).
[58] E. A. Golovchenko and A. N. Pilipetskii, J. Opt. Soc. Am. B **11**, 92 (1994).
[59] M. Yu, C. J. McKinstrie, and G. P. Agrawal, Phys. Rev. E **52**, 1072 (1995).
[60] Y. Chen, K. Beckwitt, F. Wise, B. Aiken, J. Sanghera, and I. D. Aggarwal, J. Opt. Soc. Am. B **23**, 347 (2006).
[61] M. Djoko and T. C. Kofané, Commun. Nonl. Sci. Numer. Simul. **48**, 179 (2017).
[62] K. K. Ndebele, C. B. Tabi, and T. C. Kofané, J. Opt. Soc. Am. B **37**, A214 (2020).
[63] A. J. M. Jawad, M. J. Abu-AlShaeer, E. ME Zayed, M. EM Alngar, A. Biswas, M. Ekici, A. K. Alzahrani, and M. R. Belic, Optik **223**, 165329 (2020).
[64] B. Xu, M. Yan, Z. Sun, and X. Tong, Optik **181**, 1019 (2019).
[65] A. Choudhuri and K Porsezian, Phys. Rev. A **85**, 033820 (2012).
[66] H. Woo-Pyo, Optics Commun. **213**, 173 (2002).
[67] M. Djoko and T. C. Kofané, Commun. Nonlinear Sci. Numer. Simul. **68**, 169 (2019).
[68] B. Kalithasan, K. Porsezian, P. T. Dinda, and B. A. Malomed, J. Opt. A: Pure Appl. Opt. **11**, 045205 (2009).
[69] A. Hasegawa and Y. Kodama, Proc. IEEE **69**, 1145 (1981).
[70] P. K. A. Wai, C. R. Menyuk, Y. C. Lee, and H. H. Chen, Opt. Lett. **11**, 464 (1986).
[71] A. S. Gouveia-Neto, M. E. Faldon, and J. M. Taylor, Opt. Lett. **13**, 770 (1988).
[72] N. Akhmediev and M. Karisson, Phys. Rev. A **51**, 2602 (1995).
[73] V. A. Vysloukh, Kvant. Elektron. (Moscou) **10**, 1688 (1983) [Sov. J. Quantum Electron. **13**, 1113 (1983)].
[74] K. J. Blow, N. J. Doran, and E. Cummins, Opt. Commun. **48**, 181 (1983).
[75] P. K. A. Wai, H. H. Chen, and Y. C. Lee, Phys. Rev. A **41**, 426 (1990).
[76] V. I. Karpman, Phys. Rev. E **47**, 2073 (1993).
[77] J. N. Elgin, Phys. Rev. A **47**, 4331 (1993).
[78] N. Sasa and J. Satsuma, J. Phys. Soc. Jpn. **60**, 409 (1991).
[79] R. Hirota, J. Math. Phys. **14**, 805 (1973).
[80] O. C. Wright III, Chaos, Solitons Fractals **33**, 374 (2007).
[81] A. Mussot, A. Kudlinski, E. Louvergneaux, M. Kolobov, and M. Taki, Opt. Lett. **35**, 1194 (2010).
[82] S. B. Cavalcanti, J. C. Cressoni, H. R. da Cruz, and A. S. Gouveia-Neto, Phys. Rev. A **43**, 6162 (1991).
[83] A. G. Shagalov, Phys. Lett. A **239**, 41 (1998).
[84] S. Pitois and G. Millot, Opt. Commun. **226**, 415 (2003).
[85] P. T. Dinda and K. Porsezian, J. Opt. Soc. Am. B **27**, 1143 (2010).
[86] K. K. K. Tam, T. J. Alexander, A. Blanco-Redondo, and C. M. de Sterke, Phys. Rev. A **101**, 043822 (2020).